Published in the Proceedings of the Royal Society A: Mathematical, Physical and Engineering Sciences, 471(2173):08 Jan 2015

A higher-order FEM for time-domain hydroelastic analysis of large floating bodies in inhomogeneous shallow water environment

T.K. Papathanasiou[†1], A. Karperaki[†2], E.E. Theotokoglou[†3], K.A. Belibassakis[‡]

[†]Department of Mechanics
School of Applied Mathematical and Physical Science
National Technical University of Athens
Zografou Campus 15773, Athens, Greece
[1]e-mail: papathth@gmail.com [2]e-mail: karperaki.ang@gmail.com
[3]e-mail: stathis@central.ntua.gr

‡School of Naval Architecture and Marine Engineering
National Technical University of Athens
Zografou Campus 15773, Athens, Greece
e-mail: kbel@fluid.mech.ntua.gr

Abstract

The study of wave action on large, elastic floating bodies has received considerable attention, finding applications in both geophysics and marine engineering problems. In this context, a higher-order FEM for the numerical simulation of the transient response of thin, floating bodies in shallow-water wave conditions is presented. The hydroelastic initial-boundary value problem, in inhomogeneous environment, characterized by bathymetry and plate thickness variation, is analyzed for two configurations: (i) a freely floating strip modeling an ice floe or a Very Large Floating Structure (VLFS), and (ii) a semi-fixed floating beam representing an ice shelf or shore-fast ice, both under long-wave forcing. The variational formulation of these problems is derived, along with the energy conservation principle and the weak solution stability estimates. A special higher-order finite element method is developed and applied to the calculation of the numerical solution. Results are presented and compared against established methodologies, thus validating the present method and illustrating its numerical efficiency. Furthermore, theoretical results concerning the energy conservation principle are verified, providing a valuable insight into the physical phenomenon investigated.

Keywords: hydroelastic analysis, large floating bodies, higher-order FEM, shallow-water conditions, wave-ice interaction

1. Introduction

The analysis and simulation of ocean wave-ice interaction poses a significant and challenging problem, due to its direct association with sea ice distribution and global climate change [1-3]. In fact, climate change has triggered wind intensification, as well as a significant increase in wave height and storm intensity over the last 20 years [4]. Hence, as wave trains become more energetic and ice formations weaken due to temperature rise, ocean wave excitation exhibits a heightened contribution to the demise of the summer Arctic sea ice cover [5] and to the stability or even growth of the winter Antarctic cover [6]. Furthermore, tsunami waves

have recently been identified as a potential mechanism of ice breaking; as in the case of Sulzberger Ice Shelf calving event in 2011 [7], where observational data suggest that the tsunami wave generated by the Honshu earthquake initiated the separation of large bodies of ice from the previously stable shelf.

Stability of ice shelves is vital for ice sheet mass balance and consequently for the global climate system [8]. Signs of an increasing ice shelf disintegration rate are a major concern among scientists, as climatic patterns are expected to shift due to the ensuing increase in melt water circulation and sea-level rise [9]. As mentioned above, ocean forcing acts as a trigger leading to calving or break off events of weakened ice formations. In particular, the structural integrity of ice shelves is found to be affected by infra-gravity waves [10], storm-generated swell [11] and tidal effects [12], thus associating ocean wave forcing with ice sheet mass balance. In the case of sea ice, ocean waves are shown to be inimical to saline sea ice as well. In fact, ocean waves and sea ice are bound in an autocatalytic mechanism. Intense seas can reduce sea ice formations to sludge. In turn, the decline of sea ice generates swelling, resulting in waves of even greater amplitude. The loss of sea ice deprives ice shelves of a buffer zone that absorbs wave energy and prevents ice shelf disintegration [13]. Ocean wave-ice interaction is manifested in both the break-up of pack ice and the calving of ice shelves or ice tongues [10-14]. In both cases, wave excitation adds to the inherent structural imperfections within the ice formation, while oscillatory flexural bending caused by the excitation ultimately leads to ice shelf calving or the splitting of pack ice.

Research on ocean wave-ice interaction focuses on both the study of waves passing through sea ice formations and their resultant effects on the latter. Mathematical models are distinguished between those incorporating continuous models simulating ice shelves as constrained infinite or semi-infinite bodies, extending into the ocean, and those dealing with solitary raft-like structures of finite dimensions, simulating ice floes, free to move in all directions. One of the early works, involving thin elastic plates in shallow water, can be found in Evans & Davies [15], where the problem was solved using the Wiener-Hopf technique. The response of solitary ice floes has been studied primarily in the frequency domain under harmonic excitation, while a number of works examine time-domain response of a compliant raft, also accounting for irregular wave forcing analysis [13]. Ice floes are commonly modelled as floating thin plates of arbitrary geometry, [16-17]. While the majority of works focus on the freely floating ice sheet problem, the response of a floating plate near a vertical wall has also been considered [18]. Various plate edge conditions have been examined, including a free edge and a fixed or pinned edge at the vertical wall interface. An analytical solution to the problem of a clamped semi-infinite, homogeneous, elastic plate over flat seabed has been presented in [19], while scattering waves by the edge of an ice cover have also been studied [20].

Given recent technological advances in offshore engineering, it is very difficult to ignore the fact that significant developments in the subject have been brought from the hydroelastic analysis of Very Large Floating Structures, an area that evolved in parallel with marine geophysics, as thoroughly depicted by Squire [21]. Pontoon type VLFS share the same hydrodynamic qualities with ice floes and as a result the methodologies developed for their study bear great resemblance. The foundation of both fields is set on hydroelasticity, the branch of science concerned with the response of deformable immersed bodies under sea wave excitation [22]. Applications span from ships and VLFS [22-24] to floating ice bodies [13]. Frequency domain methods, serving as primary analysis tools, are based on mesh methods [25, 26] or other techniques, as, for example, Galerkin schemes [27], Green function

[28] and eigenfunction expansion approaches [29]. Time domain analysis of elastic floating bodies allows for better treatment of irregularities in wave forcing and moving loads. In this direction, methods based on direct time integration schemes [30, 31] and Fourier transforms [32-34] have been developed. Focusing on the transient response of a freely floating body under long-wave excitation in shallow-water environment, a modal expansion technique has been developed by Sturova [35]. VLFS and ice floes are expected to span over considerable horizontal distances and thus, variable bathymetry effects could become important and have been considered by various authors. In particular, the effects of sloping seabed are examined in [36], while a fast-multipole technique is used in [37] to account for variable bathymetry. A coupled mode method has been developed by Belibassakis and Athanassoulis [38] for the hydroelastic analysis of a thin floating body over general bathymetry characterized by continuous depth variation. The latter method has been extended to weakly non-linear waves [39], and shear deformable large floating bodies of finite thickness lying over variable bathymetry regions [40]. Various attempts have been made to account for more general wave excitation, higher-order elastic plate models and treatment of geometrical complexities. In particular, methods for studying irregular wave effects, like tsunami and multidirectional ocean waves, have been developed [41-43]. Moreover, the Kirchhoff thin plate assumption which is usually considered for both VLFS and ice floes [15-17,38] has been criticized as restrictive and unrealistic, [21,22] and thus non-linear and higher-order models, like the von-Karman plate [44] and Timoshenko theory [45,46] have been incorporated and applied to hydroelastic problems involving large floating bodies.

In the present work, the finite element method will be employed for the calculation of the transient response of large floating bodies of variable thickness, under long wave excitation, in an inhomogeneous shallow water environment. In particular, in Section 2 the mathematical formulation of hydroelastic problems concerning a freely floating thin, elastic strip and a semi-fixed beam under long wave excitation are presented. Then, in Section 3, the variational formulations of the above problems are presented and, subsequently, in Section 4 the principle of energy conservation and stability estimates for the weak solution are derived and discussed. Section 5, presents the special finite element method developed for the numerical solution of the aforementioned variational problems. Finally in Section 6, numerical results based on two chosen examples are presented and discussed, illustrating the efficiency of the present method. For validation, numerical results are compared against the method developed by Sturova [35]. Finally, the main theoretical results concerning the energy conservation principle are verified, providing a valuable insight into the physical phenomenon.

2. Governing Equations

In this section the mathematical model of linear waves interacting with a floating body of small thickness, lying over variable bathymetry in shallow water conditions, is presented. For simplicity, the 2D problem on the vertical xz plane corresponding to a beam under the action of normally incident waves is treated. However the present analysis is directly extendable to the 3D problem and multidirectional wave conditions. A Cartesian coordinate system is introduced with origin at the mean water level and the z-axis pointing upwards. The plate of uniform density ρ_p and variable thickness $\tau(x)$ spans horizontally over $0 < x < L$, where L is the plate length. Additionally, the plate is assumed to extend infinitely in the transverse y-

direction. The liquid of constant density ρ_w, is confined within the variable bathymetry domain $\Omega: 0 < x < \infty$, $-H(x) < z < 0$, where $H(x)$ denotes the local water depth, measured from the still water surface. Under the irrotationality assumption, the velocity potential in the fluid region $\varphi(x,z,t)$, satisfies the Laplace equation in Ω ($\nabla^2\varphi = 0$), and the impermeable bottom boundary condition on the mildly-sloped seabed

$$\nabla\varphi \cdot \mathbf{n} = 0 \text{ on } \Gamma_b, \tag{2.1}$$

where $\mathbf{n}$ is the outer normal vector. On the free surface, the linearised condition applies

$$\partial_{tt}\varphi + g\partial_z\varphi = 0 \text{ on } \Gamma_f, \tag{2.2}$$

where g is the acceleration of gravity and $\partial_a(\bullet) \equiv \partial(\bullet)\big/\partial a$. As the plate is considered thin compared to its length scale and its wetted surface mildly sloped, the Euler-Bernoulli beam theory is adopted. Hence, on the plate boundary the dynamic and kinematic boundary conditions, respectively, are

$$m(x)\,\partial_{tt}\eta + \partial_{xx}(D(x)\,\partial_{xx}\eta) = -q(x,t) + p\ , \quad \text{and} \quad \partial_t\eta = \partial_z\varphi \text{ on } \Gamma_p, \tag{2.3}$$

where $m(x) = \rho_p\tau(x)$ is the plate mass density and $D(x) = \dfrac{E\tau^3(x)}{12(1-\nu^2)}$ the flexural rigidity, E is the Young modulus and ν denotes Poisson's ratio. Also, $q(x,t)$ is the vertical load on the plate, $\eta(x,t)$ is the deflection and $p/\rho_w = -g\eta - \partial_t\varphi$ denotes the dynamic component of pressure. The problem is supplemented by appropriate conditions at infinity and initial conditions, as follows

$$\partial_x\varphi = 0 \ \left(|x| \to \infty\right), \qquad \text{and} \qquad \eta(x,0) = \eta_0(x), \quad t=0. \tag{2.4}$$

(a) Shallow water approximation

Floating bodies of interest, in both geophysical and engineering scales, feature large horizontal dimensions compared to water depth. In polar geophysics for example, an ice shelf might extend over 100 km into the ocean, floating over a depth of only 100 m [7]. This fact renders the shallow water approximation ($\varphi(x,z,t) \approx \phi(x,t)$) valid for the problems concerning the present work. Hence, the linear shallow water equations coupled with the dynamic equation of the plate (Eq. 2.3) in the respective region, yield the system,

$$m(x)\partial_{tt}\eta + \partial_{xx}(D(x)\partial_{xx}\eta) + \rho_w g\eta + \rho_w\partial_t\phi = -q(x,t), \tag{2.5}$$

$$\partial_t\eta + \partial_x(b(x)\partial_x\phi) = 0, \tag{2.6}$$

where $b(x) = H(x) - d(x)$ is the bathymetry function incorporating the mean water depth $H(x)$ and the plate draft $d(x)$. The latter, assuming that each segment of the plate is neutrally buoyant, is $d(x) = \rho_w^{-1}\rho_p\tau(x)$ [35, 47].

Published in the Proceedings of the Royal Society A: Mathematical, Physical and Engineering Sciences, 471(2173):08 Jan 2015

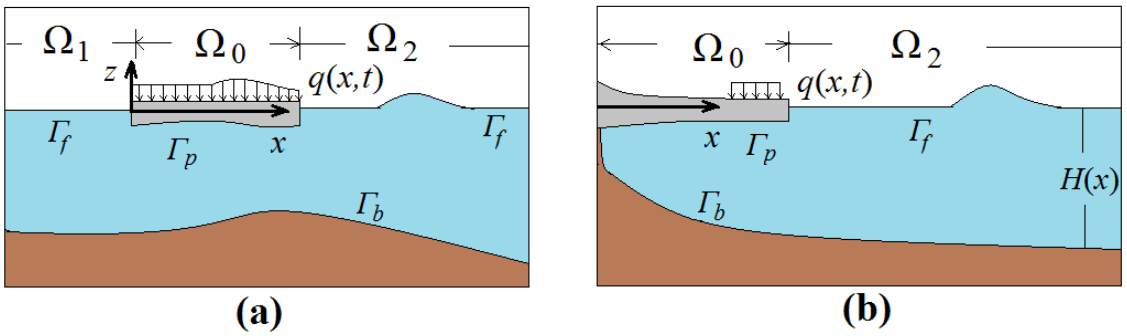

Figure 1. Configurations of hydroelastic interaction under shallow water conditions: (a) freely floating thin flexible strip, (b) floating cantilever.

Outside the floating plate region, the linear shallow water system reduces to the wave equation

$$\partial_{tt}\phi - g\partial_x(b(x)\partial_x\phi) = 0\,, \tag{2.7}$$

where $b(x) = H(x)$. The free surface elevation in this region is $\eta = -g^{-1}\partial_t\phi$.

In the following sections, two hydroelastic problems regarding to the response of thin floating bodies under long wave excitation are considered; see Fig.1. The first model problem concerns the case of a freely floating strip, while the second simulates, the response of a floating semi-fixed beam modeling the interaction of waves with shorefast ice or even an ice shelf.

(b) Freely floating, thin, flexible strip

Let $L, T \in \mathbb{R}_+$ and define the domains $\Omega_0 \equiv (0, L)$, $\Omega_1 \equiv (-\infty, 0)$, $\Omega_2 \equiv (L, +\infty)$. Using the length of the beam as a characteristic length, the following nondimensional variables are introduced: $\tilde{x} = L^{-1}x$, $\tilde{t} = g^{1/2}L^{-1/2}t$, $\tilde{\eta} = L^{-1}\eta$ and $\tilde{\phi}_i = g^{-1/2}L^{-3/2}\phi_i$, $i = 0,1,2$. The system of governing equations for a freely floating thin elastic strip is (using the nondimensional variables and dropping tildes):

$$\partial_{tt}\phi_1 - \partial_x(B(x)\partial_x\phi_1) = 0 \quad \text{in } \Omega_1 \times (0,T] \tag{2.8}$$

$$M(x)\partial_{tt}\eta + \partial_{xx}(K(x)\partial_{xx}\eta) + \eta + \partial_t\phi_0 = Q(x,t) \quad \text{in } \Omega_0 \times (0,T] \tag{2.9}$$

$$\partial_t\eta + \partial_x(B(x)\partial_x\phi_0) = 0 \text{ in } \Omega_0 \times (0,T] \tag{2.10}$$

$$\partial_{tt}\phi_2 - \partial_x(B(x)\partial_x\phi_2) = 0 \quad \text{in } \Omega_2 \times (0,T] \tag{2.11}$$

where $M(x) = \dfrac{m(x)}{\rho_w L}$, $K(x) = \dfrac{D(x)}{\rho_w g L^4}$, $B(x) = \dfrac{b(x)}{L}$ and $Q(x,t) = -\dfrac{q(x,t)}{\rho_w g L}$. The non dimensional bending moment and shear force in the flexible strip are

$$M_b(x,t) = K\partial_{xx}\eta \text{ and } V(x,t) = \partial_x(K\partial_{xx}\eta)\ . \tag{2.12}$$

The above system is supplemented with boundary, interface and initial conditions. The boundary conditions stating that both the bending moment and shear force vanishes at the ends of the strip are

$$M_b(0,t) = V(0,t) = M_b(1,t) = V(1,t) = 0\,. \tag{2.13}$$

The interface conditions expressing conservation of mass and energy at the water interface between regions Ω_1, Ω_0 and Ω_2, Ω_0 are [35, 47],

$$B(0^-)\partial_x\phi_1(0^-,t) = B(0^+)\partial_x\phi_0(0^+,t) \text{ and } \partial_t\phi_1(0^-,t) = \partial_t\phi_0(0^+,t) \tag{2.14}$$

$$B(1^-)\partial_x\phi_0(1^-,t) = B(1^+)\partial_x\phi_2(1^+,t) \text{ and } \partial_t\phi_0(1^-,t) = \partial_t\phi_2(1^+,t). \tag{2.15}$$

.

Finally, appropriate initial conditions are

$$\eta(x,0) = \phi_0(x,0) = 0\,, \text{ in } \Omega_0\,, \tag{2.16}$$

$$\phi_1(x,0) = 0, \quad \partial_t\phi_1(x,0) = 0\,, \text{ in } \Omega_1 \text{ and} \tag{2.17}$$

$$\phi_2(x,0) = 0, \quad \partial_t\phi_2(x,0) = -S(x)\,, \text{ in } \Omega_2\,. \tag{2.18}$$

where $S(x) = L^{-1}s(x)$. The generalization of the above formulation to many interacting floating strips is direct.

(c) Floating semi-fixed beam

Considering now the initial-boundary value problem for the case of floating cantilever (see also Fig. 1(b)) is given by (2.9), (2.10), and (2.11). In this case, zero deflection and rotation for the beam are assumed at $x = 0$ and the respective boundary conditions read

$$\eta(0,t) = \partial_x\eta(0,t) = M_b(1,t) = V(1,t) = 0\,, \tag{2.19}$$

Interface conditions at $x = 1$ are the same as (2.15). Assuming an impermeable wall underneath the beam at its fixed end $x = 0$, the zero velocity condition yields

$$\partial_x\phi_0(0,t) = 0\,.$$

Finally, initial conditions for this problem are given by Eqs. (2.16) and (2.18)

3. Variational formulation

In this section, the variational formulation of problems Π1 and Π2 will be presented. The following notation will be used. For every Hilbert space U, we denote by $(\cdot\,,\,\cdot)_U$ the corresponding inner product and $\|\cdot\|_U$, $|\cdot|_U$, the induced norm and seminorm, respectively. The standard notation $H^k(\Omega)$ is used for the classical Sobolev (Hilbert) spaces

$W^{k,2}(\Omega)$, $k \in \mathbb{N}$. For $T > 0$, we denote the Banach valued function spaces as $L^p(0,T;U)$, $1 \le p \le \infty$ and the corresponding norm

$$\|u\|_{L^p(0,T;U)} \doteq \left(\int_0^T \|u\|_U^p \, dt \right)^{1/p}, \; 1 \le p < \infty \text{ and } \|u\|_{L^\infty(0,T;U)} \doteq ess \sup_{t \in [0,T]} \|u\|_U .$$

Finally, $\|u\|_{C^0([0,T];U)} \doteq \max_{t \in [0,T]} \|u\|_U$ (see e.g. [48]).

(a) Variational formulation of problem Π1

In order to derive the variational formulation, Eqs. (2.9), (2.10), (2.8) and (2.11) are multiplied by $w_1 \in H^1(\Omega_1), v \in H^2(\Omega_0), -w_0 \in H^1(\Omega_0)$ and $w_2 \in H^1(\Omega_2)$, respectively. Assuming enough regularity for the proper definition of all integrals and the application of integration by parts we get

$$\int_{-\infty}^0 w_1 \partial_{tt} \phi_1 dx - \left[B w_1 \partial_x \phi_1 \right]_{-\infty}^0 + \int_{-\infty}^0 B \partial_x w_1 \partial_x \phi_1 dx = 0 \;, \tag{3.1}$$

$$\int_0^L M v \partial_{tt} \eta dx + \int_0^L (K \partial_{xx} v \partial_{xx} \eta + v \eta) dx + \int_0^L v \partial_t \phi_0 dx = \int_0^L v Q(x,t) dx \;, \tag{3.2}$$

$$-\int_0^L w_0 \partial_t \eta dx - \left[B w_0 \partial_z \phi_0 \right]_0^L + \int_0^L B \partial_x w_0 \partial_x \phi_0 dx = 0 \;, \tag{3.3}$$

$$\int_L^\infty w_2 \partial_{tt} \phi_2 dx - \left[B w_2 \partial_x \phi_2 \right]_L^\infty + \int_L^\infty B \partial_x w_2 \partial_x \phi_2 dx = 0 \;, \tag{3.4}$$

Adding (3.1)-(3.4) and using the boundary condition (2.13) and the interface conditions (2.14), (2.15), we have the following variational problem:

Find $\eta(x,t)$, $\phi_0(x,t)$, $\phi_1(x,t)$ and $\phi_2(x,t)$ such that for every $v \in H^2(\Omega_0)$, $w_0 \in H^1(\Omega_0)$, $w_1 \in H^1(\Omega_1)$ and $w_2 \in H^1(\Omega_2)$ it is

$$\begin{aligned} &\int_0^L v M \partial_{tt} \eta dx + \int_0^L v \partial_t \phi_0 dx - \int_0^L w_0 \partial_t \eta dx + \int_L^{+\infty} w_2 \partial_{tt} \phi_2 dx + \int_{-\infty}^0 w_1 \partial_{tt} \phi_1 dx + \\ &+ a(\eta, v) + b_0(w_0, \phi_0) + b_1(w_1, \phi_1) + b_2(w_2, \phi_2) = \int_0^L v Q(x,t) dx \,, \end{aligned} \tag{3.5}$$

in $(0,T]$ with initial conditions,

$$(\phi_1(x,0), w_1)_{L^2(\Omega_1)} = (\partial_t \phi_1(x,0), w_1)_{L^2(\Omega_1)} = 0 \,, \tag{3.6}$$

$$(\eta(x,0), v)_{L^2(\Omega_0)} = (\phi_0(x,0), w_0)_{L^2(\Omega_0)} = 0 \,, \tag{3.7}$$

$$(\phi_2(x,0), w_2)_{L^2(\Omega_2)} = 0, \;\; (\partial_t \phi_2(x,0), w_2)_{L^2(\Omega_2)} = -(S(x), w_2)_{L^2(\Omega_2)} . \tag{3.8}$$

For each $t \in (0,T]$, the bilinear functionals $a : H^2(\Omega_0) \times H^2(\Omega_0) \to \mathbb{R}$, $b_0 : H^1(\Omega_0) \times H^1(\Omega_0) \to \mathbb{R}$, $b_1 : H^1(\Omega_1) \times H^1(\Omega_1) \to \mathbb{R}$ and $b_2 : H^1(\Omega_2) \times H^1(\Omega_2) \to \mathbb{R}$ are defined as

$$a(\eta, v) = \int_0^L (K\partial_{xx} v \partial_{xx} \eta + v\eta) dx, \quad b_0(w_0, \phi_0) = \int_0^L B\partial_x w_0 \partial_x \phi_0 dx, \tag{3.9}$$

$$b_1(w_1, \phi_1) = \int_{-\infty}^0 B\partial_x w_1 \partial_x \phi_1 dx, \; b_2(w_2, \phi_2) = \int_L^\infty B\partial_x w_2 \partial_x \phi_2 dx. \tag{3.10}$$

(b) Variational formulation of problem Π2

In this case, the appropriate solution space is

$$V = \quad u \in H^2(\Omega_0) \,|\, u(0) = \partial_x u(0) = 0 \quad .$$

Similarly to the variational formulation of problem Π1, and using the corresponding boundary and interface conditions presented in Sec. 2(c), we have the following formulation:

Find $\eta(x,t)$, $\phi_0(x,t)$ and $\phi_2(x,t)$ such that for every $v \in V$, $w_0 \in H^1(\Omega_0)$ and $w_2 \in H^1(\Omega_2)$ it is,

$$\begin{aligned} &\int_0^L vM\partial_{tt}\eta dx + \int_0^L v\partial_t \phi_0 dx - \int_0^L w_0 \partial_t \eta dx + \int_L^{+\infty} w_2 \partial_{tt} \phi_2 dx \\ &+ a(\eta, v) + b_0(w_0, \phi_0) + b_2(w_2, \phi_2) = \int_0^L vQ(x,t) dx \end{aligned}, \tag{3.11}$$

in $(0,T]$ with initial conditions,

$$(\eta(x,0), v)_{L^2(\Omega_0)} = (\phi_0(x,0), w_0)_{L^2(\Omega_0)} = 0 \quad , \tag{3.12}$$

$$(\phi_2(x,0), w_2)_{L^2(\Omega_2)} = 0, \;\; (\partial_t \phi_2(x,0), w_2)_{L^2(\Omega_2)} = -(S(x), w_2)_{L^2(\Omega_2)}. \tag{3.13}$$

4. Energy conservation and stability estimates

In this section, under the assumption of sufficient regularity for the weak solutions of the variational problems presented in the previous section, an energy conservation principle will be derived, along with stability estimates for the weak solution of problems Π1 and Π2. The respective propositions will be derived for both the freely floating beam and the floating cantilever simultaneously.

The following assumptions are introduced, where for problem Π2 we set $\Omega_1 \equiv \varnothing$.

(A1) $S(x) \in H^1(\Omega_2)$.

(A2) Let $X \equiv \bigcup_{i=0,1,2} \Omega_i$. For the bathymetry function it is $B \in L^\infty(X)$. We denote, $C_B = \left\| B(x) \right\|_{L^\infty(X)}$ and assume there exists positive constant c_B such that $ess \inf_{x \in X} B(x) \geq c_B > 0$. That is, the bathymetry attains only positive values so that the seabed never reaches the water free surface in Ω_1, Ω_2 and the lower surface of the ice self in Ω_0.

(A3) It is $M, K \in L^\infty(\Omega_0)$ and there exists positive constants c_M, c_K such that $ess \inf_{x \in \Omega_0} M(x) \geq c_M > 0$ and $ess \inf_{x \in \Omega_0} K(x) \geq c_K > 0$.

(A4) For the solution of problem Π1, it is assumed that $\eta, \partial_t \eta \in L^2(0,T;H^2(\Omega_0))$, $\partial_{tt}\eta \in L^2(0,T;L^2(\Omega_0))$ and $\phi_i, \partial_t \phi_i \in L^2(0,T;H^1(\Omega_i))$, $\partial_{tt}\phi_i \in L^2(0,T;L^2(\Omega_i))$ $i = 0,1,2$.

The solution of problem Π2 is assumed to satisfy $\eta, \partial_t \eta \in L^2(0,T;V)$, $\partial_{tt}\eta \in L^2(0,T;L^2(\Omega_0))$ and $\phi_i, \partial_t \phi_i \in L^2(0,T;H^1(\Omega_i))$, $\partial_{tt}\phi_i \in L^2(0,T;L^2(\Omega_i))$ $i = 0,2$.

The first main result is presented in the following subsection, for both configurations.

(a) Energy conservation principle

Let $\lambda = 1$ when the variational problem under consideration is Π1 and $\lambda = 0$ for problem Π2, and define the quantity

$$E(t;\lambda) \doteq \left\| M^{1/2} \partial_t \eta \right\|^2_{L^2(\Omega_0)} + \lambda \left\| \partial_t \phi_1 \right\|^2_{L^2(\Omega_1)} + \left\| \partial_t \phi_2 \right\|^2_{L^2(\Omega_2)} + a(\eta,\eta) + b_0(\phi_0,\phi_0) + \lambda b_1(\phi_1,\phi_1) + b_2(\phi_2,\phi_2) \quad . \tag{4.1}$$

The following theorem states an energy conservation principle for problems Π1 and Π2.

Theorem 1 (Energy conservation principle). Let $Q \equiv 0$ and assume that **(A1), (A2), (A3)** and **(A4)** hold. Then, $\forall t \in (0,T]$ it is $E(t;\lambda) = E(0;\lambda)$.

Proof. For problem Π1, set $v = \partial_t \eta, w_0 = \partial_t \phi_0, w_1 = \partial_t \phi_1, w_2 = \partial_t \phi_2$ in (3.1), (3.2), (3.3) and (3.4). For problem Π2 set $v = \partial_t \eta, w_0 = \partial_t \phi_0, w_2 = \partial_t \phi_2$ in (3.11). In both cases,

$$-\int_0^L \partial_t \eta \partial_t \phi_0 dx + \int_0^L \partial_t \phi_0 \partial_t \eta dx = 0, \tag{4.2}$$

is directly achieved. In the same time all boundary terms appearing in those equations vanish due to the interface conditions Eqs. (2.13)-(2.15) and (2.19). By invoking the assumed regularity, the following relations hold

$$\int_0^L M \partial_{tt}\eta \partial_t \eta dx = \frac{1}{2}\frac{d}{dt}\left\| M^{1/2}\partial_t \eta \right\|^2_{L^2(\Omega_0)}, \int_{-\infty}^0 \partial_{tt}\phi_1 \partial_t \phi_1 dx = \frac{1}{2}\frac{d}{dt}\left\| \partial_t \phi_1 \right\|^2_{L^2(\Omega_1)}, \int_L^{+\infty} \partial_{tt}\phi_2 \partial_t \phi_2 dx = \frac{1}{2}\frac{d}{dt}\left\| \partial_t \phi_2 \right\|^2_{L^2(\Omega_2)} \tag{4.3}$$

and

$$a(\partial_t\eta,\eta)=\int_0^L K\partial_{txx}\eta\partial_{xx}\eta dx+\int_0^L\partial_t\eta\eta dx=\frac{1}{2}\frac{d}{dt}a(\eta,\eta) \tag{4.4}$$

Similarly it is

$$\begin{aligned} b_0(\partial_t\phi_0,\phi_0)=\frac{1}{2}\frac{d}{dt}b_0(\phi_0,\phi_0), b_1(\partial_t\phi_1,\phi_1)=\frac{1}{2}\frac{d}{dt}b_1(\phi_1,\phi_1)\\ b_2(\partial_t\phi_2,\phi_1)=\frac{1}{2}\frac{d}{dt}b_2(\phi_2,\phi_2)\end{aligned} \tag{4.5}$$

Using (4.3), (4.4) and (4.5) we derive in compact form for problems Π1 and Π2

$$\begin{aligned}&\frac{d}{ds}\left[\left\|M^{1/2}\partial_s\eta(s)\right\|^2_{L^2(\Omega_0)}+\lambda\left\|\partial_s\phi_1(s)\right\|^2_{L^2(\Omega_1)}+\left\|\partial_s\phi_2(s)\right\|^2_{L^2(\Omega_2)}\right]+\frac{d}{ds}\left[a(\eta(s),\eta(s))\right]\\&+\frac{d}{ds}\left[b_0(\phi_0(s),\phi_0(s))+\lambda b_1(\phi_1(s),\phi_1(s))+b_2(\phi_2(s),\phi_2(s))\right]=2\int_0^L\partial_s\eta Q(x,s)dx\end{aligned} \tag{4.6}$$

Setting $Q=0$, integrating (4.6) with respect to time from $s=0$ to $s=t$ and using initial conditions (3.6)-(3.8), (3.12), (3.13) the conservation of $E(t;\lambda)$ is obtained. □

Equation (4.1) is an energy conservation principle, which states that when no forcing is present, the total hydroelastic energy, i.e. the kinetic and strain energy of the beam along with the kinetic and potential energy of the water column remains constant in time and equals the energy of the initial water free surface elevation in the region outside the hydroelastic interaction.

Remark: The bathymetry function B, possesses a discontinuity in the form of a finite jump at $x=L$. Thus, when defined as a function $B:X\to\mathbb{R}_+$ the regularity $B\in L^\infty(X)$ is appropriate in order to form a simple but realistic model. However, the bathymetry function could be smoother when restricted to the interior of Ω_0 ,Ω_1 and Ω_2. In fact, higher regularity for these restrictions of the bathymetry function and M,K,S is typically needed in order to ensure the solution spaces described in **(A4).**

(b) Stability estimates for the flexible strip response

Stability estimates, in the physical energy norm for the hydroelastic problem, will be derived. In addition, a priori estimates for the ice self deformation characteristics in the maximum norm will be proven.

Theorem 2. Let assumptions **(A1)**, **(A2)**, **(A3), (A4)** hold. Further let $Q\in L^2(0,T;L^2(\Omega_0))$. Then there exists constant $C\in\mathbb{R}_+$ such that

$$\begin{aligned}&\left\|\partial_t\eta\right\|^2_{L^2(\Omega_0)}+\left\|\eta\right\|^2_{H^2(\Omega_0)}+\left|\phi_0\right|^2_{H^1(\Omega_0)}+\left\|\partial_t\phi_2\right\|^2_{L^2(\Omega_2)}+\left|\phi_2\right|^2_{H^1(\Omega_2)}\\&+\lambda\left\|\partial_t\phi_1\right\|^2_{L^2(\Omega_1)}+\lambda\left|\phi_1\right|^2_{H^1(\Omega_1)}\le C^{-1}e^{C^{-1}T}\left(\left\|S\right\|^2_{L^2(\Omega_2)}+\left\|Q\right\|^2_{L^2(0,T;L^2(\Omega_1))}\right),\end{aligned} \tag{4.7}$$

Proof. Integrating (4.5) with respect to time from $s=0$ to $s=t$ and using initial conditions, we get,

$$\begin{aligned}&\left\|M^{1/2}\partial_t\eta\right\|^2_{L^2(\Omega_0)}+\lambda\left\|\partial_t\phi_1\right\|^2_{L^2(\Omega_1)}+\left\|\partial_t\phi_2\right\|^2_{L^2(\Omega_2)}+a(\eta,\eta)\\&+b_0(\phi_0,\phi_0)+\lambda b_1(\phi_1,\phi_1)+b_2(\phi_2,\phi_2)=\left\|S\right\|^2_{L^2(\Omega_2)}+2\int_0^t\int_0^L\partial_s\eta Q(x,s)dxds\end{aligned}. \quad (4.8)$$

Using Cauchy-Schwarz inequality and inequality $2\kappa\mu\le\kappa^2+\mu^2$ for real numbers it is,

$$\left|\int_0^L\partial_s\eta Q dx\right|\le\frac{1}{2}\int_0^L(\partial_s\eta)^2+Q^2\ dx=\frac{1}{2}\left\|\partial_s\eta\right\|^2_{L^2(\Omega_0)}+\frac{1}{2}\left\|Q\right\|^2_{L^2(\Omega_0)}. \quad (4.9)$$

Invoking **(A3)** it is, $\left\|M^{1/2}\partial_t\eta\right\|^2_{L^2(\Omega_0)}\ge c_M\left\|\partial_t\eta\right\|^2_{L^2(\Omega_0)}$. For the bilinear functional $a(\eta,\eta)$ it is

$$a(\eta,\eta)=\int_0^L K\ \partial_{xx}\eta\ ^2dx+\int_0^L\eta^2dx\ge c_K\left|\eta\right|^2_{H^2(\Omega)}+\left\|\eta\right\|^2_{L^2(\Omega)}. \quad (4.10)$$

The norm equivalence in $H^2(\Omega_0)$ and (4.9) lead to $a(\eta,\eta)\ge c_0\min\ 1,c_K\ \left\|\eta\right\|^2_{H^2(\Omega_0)}$, for a positive constant c_0. Set $c_L=c_0\min\ 1,c_K$. Finally it is $b_i(\phi_i,\phi_i)\ge c_B\left|\phi_i\right|^2_{H^1(\Omega_i)}$, $i=0,1,2$.

From relations (4.7)-(4.10) it is

$$\begin{aligned}&\left\|\partial_t\eta\right\|^2_{L^2(\Omega_0)}+\lambda\left\|\partial_t\phi_1\right\|^2_{L^2(\Omega_1)}+\left\|\partial_t\phi_2\right\|^2_{L^2(\Omega_2)}+\left\|\eta\right\|^2_{H^2(\Omega_0)}+\left|\phi_0\right|^2_{H^1(\Omega_0)}\\&+\lambda\left|\phi_1\right|^2_{H^1(\Omega_1)}+\left|\phi_2\right|^2_{H^1(\Omega_2)}\le C^{-1}\left(\left\|S\right\|^2_{L^2(\Omega_2)}+\int_0^t\left\|\partial_s\eta\right\|^2_{L^2(\Omega_0)}ds+\int_0^t\left\|Q(x,s)\right\|^2_{L^2(\Omega_0)}ds\right)\end{aligned} \quad (4.11)$$

where $C=\min\ 1,c_M,c_L,c_B$. Application of Gronwall's lemma in (4.11) yields the desired result. □

We now proceed to the derivation of a stability estimate for the elastic strip deflection field in the appropriate energy norm

Theorem 3. Let all assumptions stated in Theorem 2 hold. Then it is

$$\left\|\partial_t\eta\right\|_{L^2(0,T;L^2(\Omega_0))}+\left\|\eta\right\|_{L^2(0,T;H^2(\Omega_0))}\le\sqrt{2C^{-1}Te^{C^{-1}T}}\ \left\|S\right\|_{L^2(\Omega_2)}+\left\|Q\right\|_{L^2(0,T;L^2(\Omega_0))}, \quad (4.12)$$

with $C=\min\ 1,c_M,c_L,c_B$

Proof. From Theorem 2 we get

$$\left\|\partial_t\eta\right\|^2_{L^2(\Omega_0)}+\left\|\eta\right\|^2_{H^2(\Omega_0)}\le C^{-1}e^{C^{-1}T}\left(\left\|S\right\|^2_{L^2(\Omega_2)}+\left\|Q\right\|^2_{L^2(0,T;L^2(\Omega_2))}\right), \quad (4.13)$$

where $C = \min\ 1, c_M, c_K c_L, c_W^{-2} c_B$. Integrating with respect to time in $[0,T]$

$$\left\|\partial_t \eta\right\|^2_{L^2(0,T;L^2(\Omega_0))} + \left\|\eta\right\|^2_{L^2(0,T;H^2(\Omega_0))} \leq C^{-1} T e^{C^{-1}T} \left(\left\|S\right\|^2_{L^2(\Omega_2)} + \left\|Q\right\|^2_{L^2(0,T;L^2(\Omega_0))} \right). \qquad (4.14)$$

Taking square roots and using the norm equivalence in $\mathbb{R}^2$ equation (4.14) yields (4.12). □

For several applications it is of interest to derive a bound on the maximum value of the flexible strip deflection and slope. For this purpose, the following classic embedding result will be used [49].

Lemma 1. Let $\Omega \subset \mathbb{R}^n$ be a Lipschitz domain. It is $W^{k,p}(\Omega) \hookrightarrow C^{\ell}(\bar{\Omega})$ if $k - \ell > np^{-1}$.

Using Theorem 2 and lemma 1, we get

Theorem 4. Let all assumptions stated in Theorem 2 hold. Then $\eta \in C^0([0,T]; C^1(\bar{\Omega}_0))$ and there exists $C_0 \in \mathbb{R}_+$

$$\left\|\eta\right\|_{C^0([0,T];C^1(\bar{\Omega}_0))} \leq \Sigma \left\|S\right\|_{L^2(\Omega_2)} + \left\|Q\right\|_{L^2(0,T;L^2(\Omega_0))}, \qquad (4.15)$$

where $\Sigma = C_0^{-1} \sqrt{C^{-1} e^{C^{-1}T}}$.

Proof . The first part follows directly from Lemma 1 and **(A4)**. From (4.7), and Lemma 1, it is

$$C_0^2 \left\|\eta\right\|^2_{C^1(\bar{\Omega}_0)} \leq C^{-1} e^{C^{-1}T} \left(\left\|S\right\|^2_{L^2(\Omega_2)} + \left\|Q\right\|^2_{L^2(0,T;L^2(\Omega_0))} \right), \qquad (4.16)$$

Thus it holds

$$\max_{t\in[0,T]} \left\|\eta\right\|^2_{C^1(\bar{\Omega}_0)} \leq C_0^{-2} C^{-1} e^{C^{-1}T} \left(\left\|S\right\|^2_{L^2(\Omega_1)} + \left\|Q\right\|^2_{L^2(0,T;L^2(\Omega_0))} \right), \qquad (4.17)$$

and (4.15) follows by taking square roots. □

5. The Finite Element Method

In this section, the discretization of the variational problems (3.5) and (3.11) with finite elements is described. A special hydroelastic element HELFEM(5,4) is introduced. The element incorporates cubic Hermite shape functions for the approximation of the beam deflection/upper surface elevation in Ω_0 (η and $\partial_x \eta$ degrees of freedom - dof) and quadratic Lagrange shape functions for the approximation of ϕ_0; see, e.g., [50,51]. The approximation spaces are defines as,

Published in the Proceedings of the Royal Society A: Mathematical, Physical and Engineering Sciences, 471(2173):08 Jan 2015

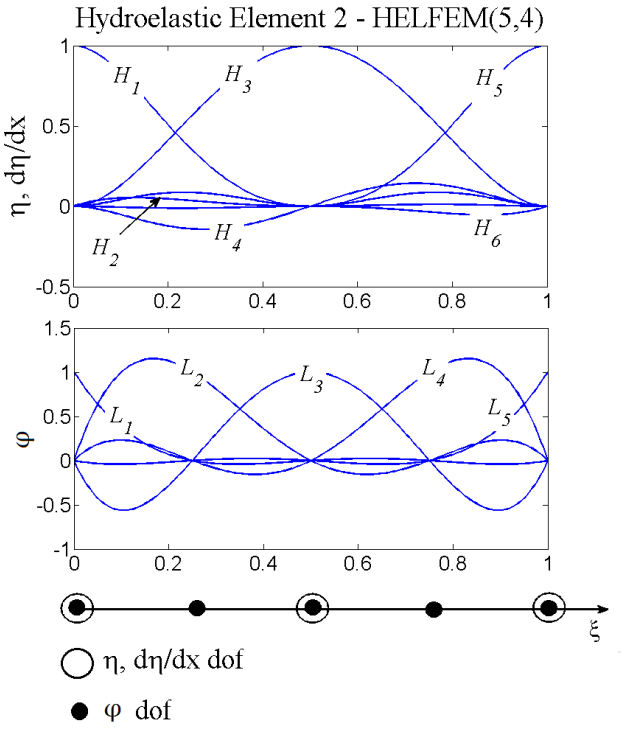

Figure 2. Shape functions of hydroelastic element HELFEM (5,4).

$$U^h = \left\{ \eta^h \mid \eta^h \in U \ (U \equiv H^2(\Omega_0) \ if \ \lambda = 1, U \equiv V \ if \ \lambda = 0) \ and \ \eta^h\Big|_e = \sum_{i=1}^{6} H_i(x)\eta_i^h(t) \right\}, \tag{5.1}$$

$$W^h = \left\{ \phi_0^h \mid \phi_0^h \in H^1(\Omega_0) \ \ and \ \phi_0^h\Big|_e = \sum_{i=1}^{5} L_i(x)\phi_{0i}^h(t) \right\}, \tag{5.2}$$

where $u^h\Big|_e$ denotes the restriction of u^h in element e, $H_i(x)$ are Hermite polynomial shape functions of order 5 and $L_i(x)$ Lagrange polynomial shape functions of order 4. For the approximation of ϕ_i in Ω_i for $i = 1, 2$, it is

$$W_i^h = \left\{ \phi_i^h \mid \phi_i^h \in H^1(\Omega_i) \ \ and \ \phi_i^h\Big|_e = \sum_{j=1}^{5} L_j(x)\phi_{ij}^h(t) \right\}. \tag{5.3}$$

The hydroelastic element shape functions are shown in Fig. 2.

(a) Discretization of the hydroelastic system

The discretization of the problem leads to a second order system of ordinary differential equations of the form

$$\mathbf{M}\partial_{tt}\mathbf{u} + \mathbf{C}\partial_t\mathbf{u} + \mathbf{K}\mathbf{u} = \mathbf{F}, \tag{5.4}$$

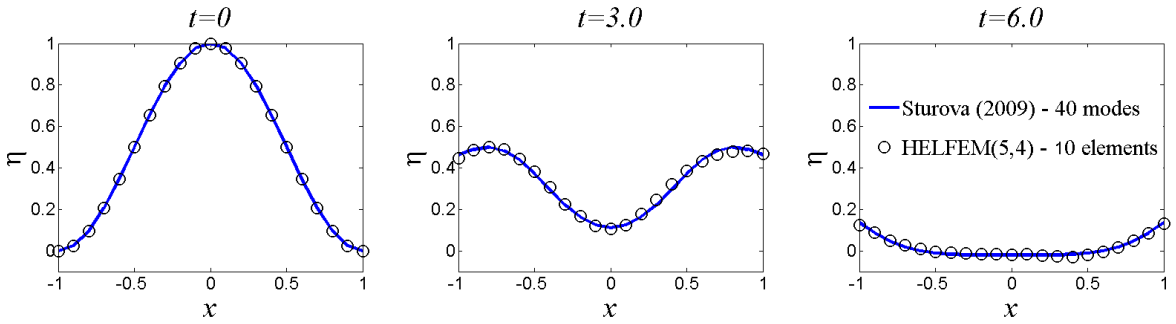

Figure 3. Comparison between the finite element solution and the method presented in [35].

where the vector of unknowns **u** contains the nodal values for η^h, ϕ_0^h, ϕ_1^h and ϕ_2^h. We remark here that matrix **M** is singular as only the term $\int_0^L v^h M \partial_{tt} \eta^h dx$ produces non zero terms in it. This fact, forces the use of an implicit time marching scheme for the integration of system (5.4). Setting $\partial_t \mathbf{u} = \mathbf{v}$, Eq.(5.4) is transformed to a first order system. Time integration of the latter first order system is performed by means of the Crank-Nicolson method [51].

(b) Validation of the present Finite Element Method

A modal expansion technique has been developed by Sturova [35] for the determination of the transient response of a freely floating, thin and heterogeneous elastic beam. The present finite element code was compared against the aforementioned technique, in an example of initial beam deflection given in [35]. Water depth was considered to be constant at 20 meters, the length of the plate was taken 500 m, while its thickness varies as $\tau(x) = 1 + 2x$. The initial deflection was of the form $\eta_0 = 0.5 + 0.5\cos(x - 5)$. The excellent agreement of the present finite element scheme for the beam deflection, employing 10 HELFEM(5,4) elements and the modal expansion technique, based on the first 40 modes, is shown in Fig. 3.

The higher order hydroelastic finite element HELFEM (5,4) exhibits rapid convergence, as expected, due to the increased degree of interpolation. Although the modal expansion method of Sturova is tailor-made for the given problem and thus yields rapid convergence, the higher–order FEM method is also found to be robust and greatly efficient. Extensive investigation of convergence characteristics and error estimates for the HELFEM schemes will be presented in a forthcoming work.

6. Numerical Results

In this section, two examples will be considered for the analysis and discussion of problems Π_1 and Π_2. In both cases a mollified Heaviside function is used as the initial upper surface elevation in the free water region. The pulse form is,

$$\eta_0 = A \exp\left(-x^{-\mu(x_0+w)^2} - x^{-\mu(x-x_0+w)(x-x_0-w)}\right), \tag{6.1}$$

where x_0 is the point of origin, w is the half length of the disturbance, A is the amplitude of the initial pulse and μ is a positive parameter controlling the smoothness (see also Fig. 4).

The initial elevation described above, simulates a dislocation generated tsunami as discussed in [52, 53]. Decreasing μ, the excitation assumes a bell-like shape, while as the latter parameter increases a step function is generated. The material properties of ice [35] are given as follows: Young's modulus of $E = 5 \times 10^9\ Pa$, Poisson's ratio $v = 0.3$, and density $\rho_i = 922.5\ kg\, m^{-3}$. Water density is taken as $\rho_w = 1025\, kg\, m^{-3}$.

(a) Freely floating strip

First we consider the case of a freely floating strip, with a uniform thickness of 4 m and length of 1 km, as shown in Fig. 4. This configuration simulates large, freely floating bodies resembling both ice floes and VLFS. A constant depth of 10 and 20 meters is assumed for regions Ω_1 and Ω_2, respectively. The plate floats over linearly varying bathymetry characterised by a constant bed slope equal to 1%. For the approximation of the plate response shown in Fig. 4, 100 HELFEM(5,4) and 10000 time steps are employed.

The space – time plot of the calculated wave field is illustrated in Fig. 4, while Fig. 5 shows the upper surface elevation at specific moments in time. We clearly observe the disintegration of the initial pulse of bandwidth $w = 100\, m$, amplitude $A = 0.2\, m$ and $\mu = 50$, into two propagating waves, in accordance to the solution of the wave equation in the constant depth region Ω_2.The two pulses travel away from the original formation, in opposite directions. As one of the travelling waves impacts the plate, partial reflection is observed. After the impact, the hydroelastic wave begins to develop in the plate, exhibiting dispersive characteristics that are clearly observed in both figures as smaller amplitude waves preceding the main disturbance. The wave train exiting the plate region, is shown to propagate into the shallower water region Ω_1, with a lower speed compared to the wave disturbance propagating in Ω_2, due to the decreased water depth. An important aspect of the present method is the ability to provide useful information concerning possible locations of high stresses and initial crack development. Both features are especially important in both the study of crack propagation and ice floe breaking or separation. In this direction, revisiting the previous example, the extreme values of bending moment and shear force at every moment in time, along with their location on the floating elastic strip are shown in Fig. 6. As it can be seen, the maximum values occur moments before the transmission of the main excitation from the plate into the free water region at the left side of the floating body.

Energy conservation, for the case of a freely floating strip, is investigated in detail in Fig. 7. Calculations by the presented FEM are found to be in perfect agreement with the theoretical analysis given in Sec.3. The total non-dimensional energy remains constant in time, as expected, since dissipation effects are not present.

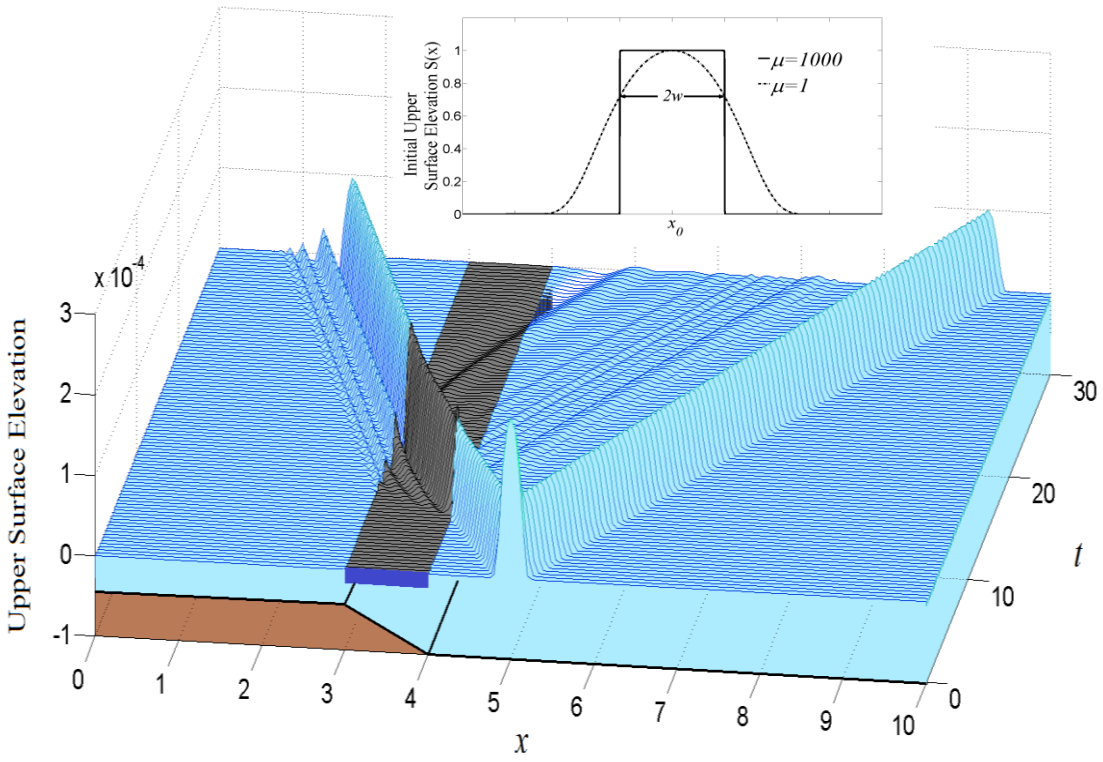

Figure 4. Space-time plot of wave propagation, for the freely floating strip example. The form of initial upper surface elevation (propagating pulse) is shown in the subplot, where w is the bandwidth and μ the form parameters.

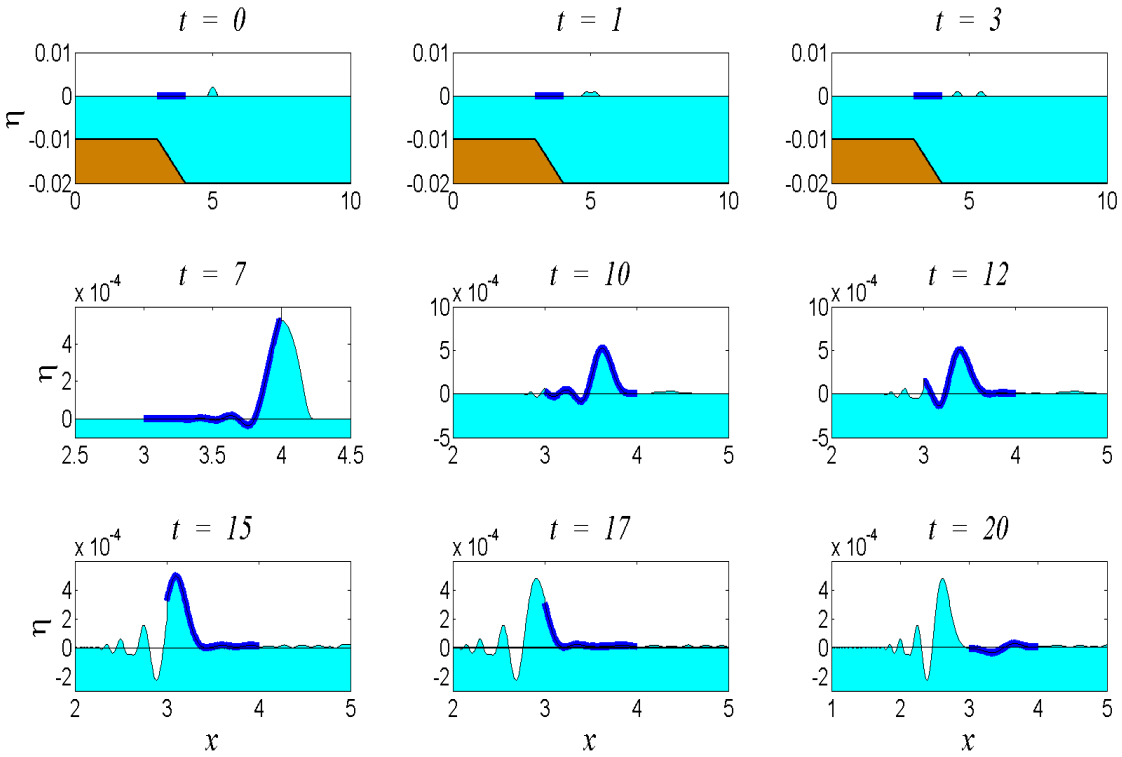

Figure 5. Calculated upper surface elevation at distinct moments. The elastic deformation of the strip is shown by a thick line (the upper surface elevation is exaggerated).

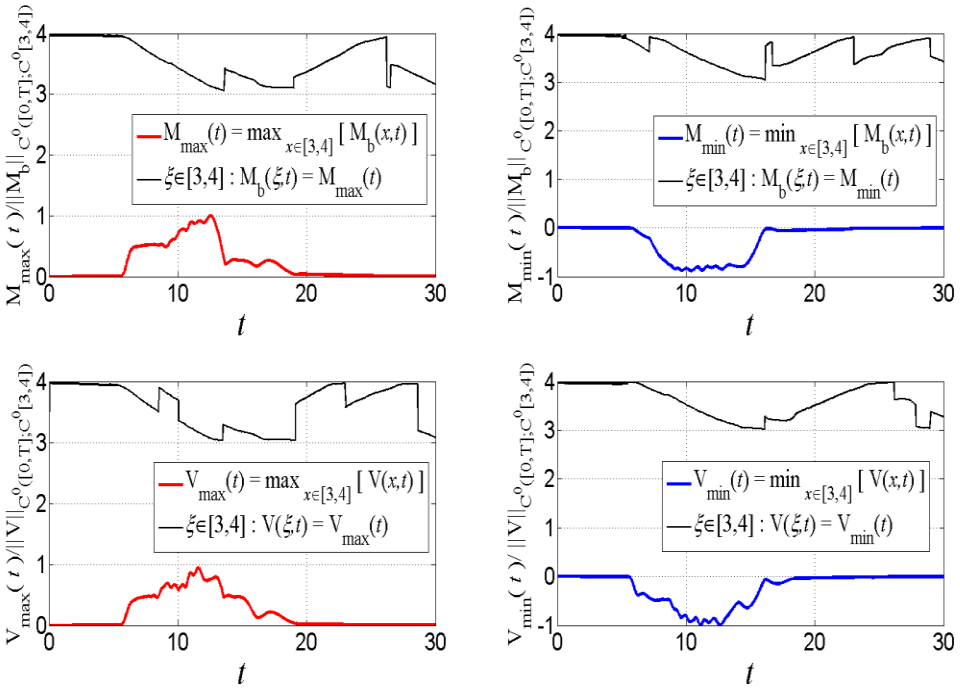

Figure 6. Extreme (max/min) values of bending moment and shear force and their location on the floating elastic strip in the case of the first example.

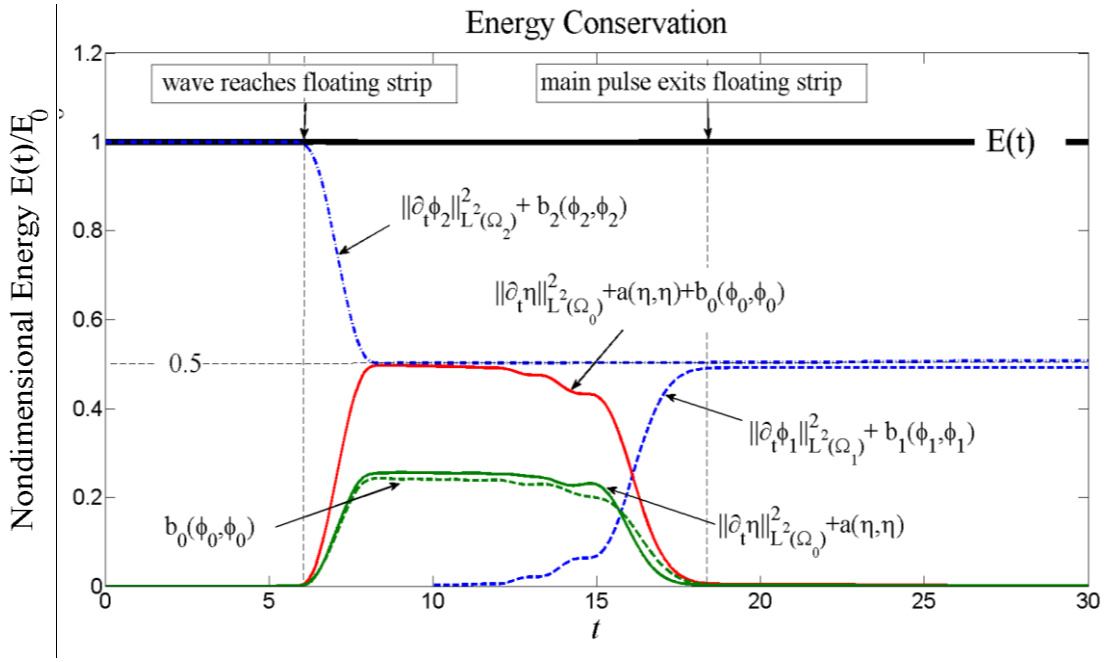

Figure 7. Illustration of the energy conservation principle, in the case of the first example. All energy quantities in the plot are nondimensionalised with respect to the initial energy of the travelling pulse E_0.

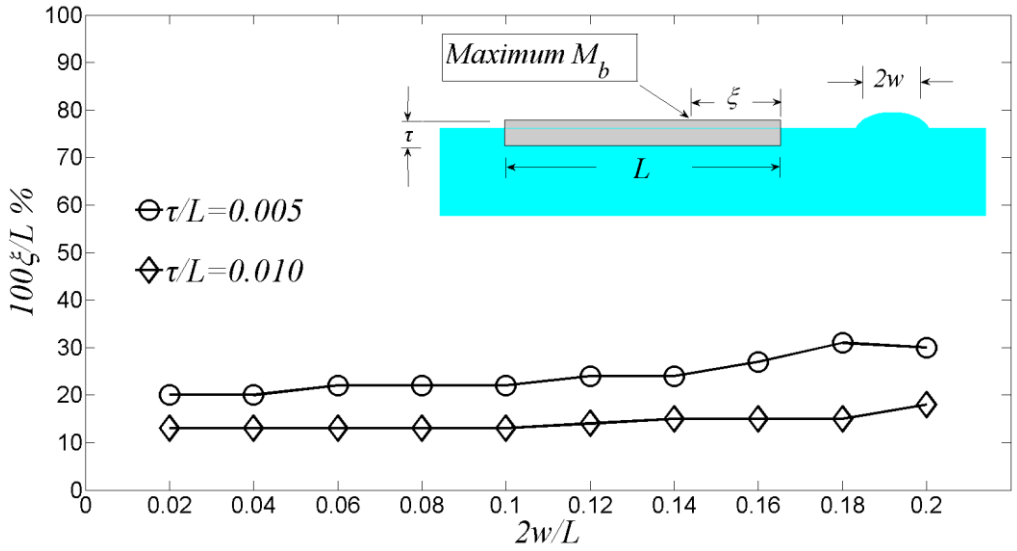

Figure 8. Location of extreme bending moment on the floating body for various values of the beam thickness and bandwidth parameters of the initial propagating disturbance (pulse).

In Fig. 7, it is observed that, at the beginning of wave motion, the total energy of the system associated with the initial pulse is confined within the water region Ω_2. At the initial moments of wave motion, the total energy amounts to the sum of the kinetic energy of the free water surface and the potential energy associated with flux discharge in region Ω_2. When the excitation reaches the floating strip ($t \simeq 5.5$) the energy flows into Ω_0, hence the strain and kinetic energy of the body, along with the discharge flux energy of the region Ω_0, increase. As the excitation transmits into Ω_1 ($t \simeq 10$), an increase in the energy of the domain can be seen, expressed as an increase of the kinetic energy of the free water surface and the discharge energy flux of the region. The energy transfer from the main pulse into the formation of smaller dispersed waves, preceding the main disturbance in Ω_1, is visible as sudden drops in the kinetic and strain energy, as well as in the flux discharge energy of region Ω_0 ($t \simeq 13,14$). When maximum bending moment occurs, the strain energy term increases momentarily, while the discharge flux energy of the region is seen to mirror the fluctuations. Gradually, as the elastic strip reaches a state of rest , the total energy of the system is given by the potential flux discharge and kinetic energies of the freely propagating waves in the water subregions Ω_2 and Ω_1.

Based on the above analysis, it is concluded that the present method is able to provide useful information concerning the distribution of stresses in a floating elastic body. Furthermore, it may contribute to the parameterization of wave ice interaction processes incorporated in global environmental models aiming at the prediction of breaking and demise events of floating ice bodies. Revisiting the freely floating configuration, the location of extreme bending moment values along the strip, for different values of beam thickness and initial pulse bandwidth are presented in Fig.8. In the analysis, the examined configuration of 20 km in length is comparable to the lateral dimensions of the B-31 iceberg, formed by calving of the Pine Island Bay glacier in Antarctica (2013) [54]. Two different (constant) thickness values have been examined, namely 0.5% and 1% of length, respectively. Finally, the depth

to length ratio is 2%. The smoothing parameter is set $\mu = 100$. It is observed (Fig. 8) that the extreme values of the bending moment are relatively insensitive to the forcing pulse wavelength especially for the shorter wavelengths of the examined pulses (these values are close to the limits of the long wave approximation). This is in agreement with the analytical result of Squire [14] on the maximum hydroelastic normal stresses on semi-infinite strips, valid for all wavelengths.

(b) Semi-fixed floating beam

The case of a semi-fixed floating beam is considered. The configuration serves as a macroscopic, mechanical model of a floating glacier under long-wave forcing; see, e.g., Sergienko [55]. In the following example, the semi-fixed floating beam, with 50 km length, resembles an ice shelve extending into the ocean, subjected to long wave-forcing. The model is able to simulate the energy transfer from an incoming tsunami wave into the ice-shelf and calculate its response to the excitation. The thickness of the beam varies linearly from 200 m at the fixed boundary to 100 m at the free end. A constant depth of 300 m is assumed for region Ω_2. A 0.1% sloping bottom is assumed under the elastic beam, reaching a depth of 250 m underneath the fixed edge. The system is subjected to the same initial wave forcing profile as the one considered in the first example. The selected parameters are $w = 2000\,m$, amplitude $A = 0.5\,m$ and $\mu = 50$

The space – time plot of the calculated wave field by the present FEM is shown in Fig. 9, while Fig. 10 shows the upper surface elevation at specific time instances. The response of the semi-fixed beam was approximated by 120 elements HELFEM (5,4), and 10000 time increments were used for the simulation shown in these figures. At $t \simeq 10$ the incident wave on the beam is partially reflected at the free tip, and the hydroelastic wave starts to develop. After some time, the waveform reaches the fixed end of the beam where it is fully reflected, and then it backpropagates into the hydroelasticity-dominated region. Finally, the wave fully reflects back into the water region, travelling away from the beam in Ω_2. The dispersive characteristics of the hydroelastic wave are clearly observed in both figures.

The extreme values of bending moment and shear force along with their location in the semi-fixed beam, are plotted in Fig. 11. In this case, it is observed that the maximum values occur at the fixed end of the beam, at the moment of full reflection, as expected by the present idealised model. However, in more realistic cases of wave - ice interaction, the effects of diffraction and dissipation, in conjunction with long propagation distances, are expected to reduce the wave action propagating towards the shore. Thus, the critical conditions for ice breakup would be rather similar to the ones arising from the previous discussion of Fig. 8.

Finally, the principle of energy conservation in the case of the second example is illustrated in Fig. 12. The reflection of the dispersed hydroelastic wave is seen in this figure as a series of fluctuations in the strain energy of the beam, due to the momentary increase in the maximum bending moment as the wave train reaches the fixed boundary. As before, the discharge flux energy in region Ω_0 is seen to mirror those fluctuations. As the reflected hydroelastic waves re-enter the sub region Ω_2, the energy of the region is seen to increase. Finally, as the excitation propagates away from the free end of the semi-fixed beam, the elastic body and the water column underneath it reach a state of rest and the total energy of

the system is given by the potential flux discharge and kinetic energies of the freely propagating wave in the water sub region Ω_2.

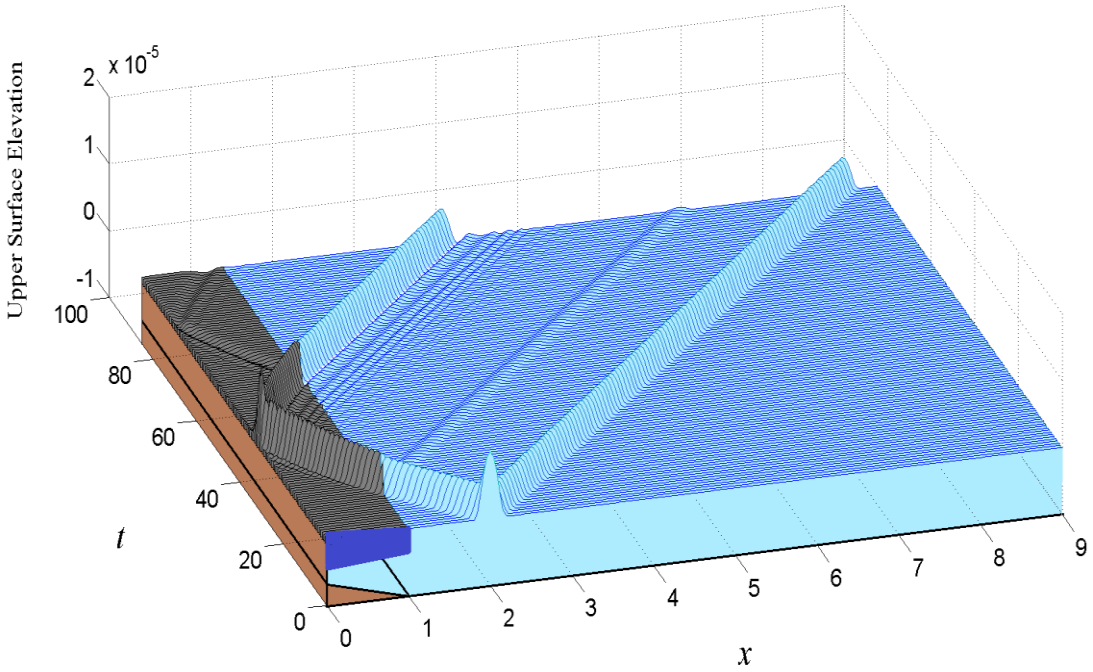

Figure 9. Space-time plot of wave propagation in the case of second example.

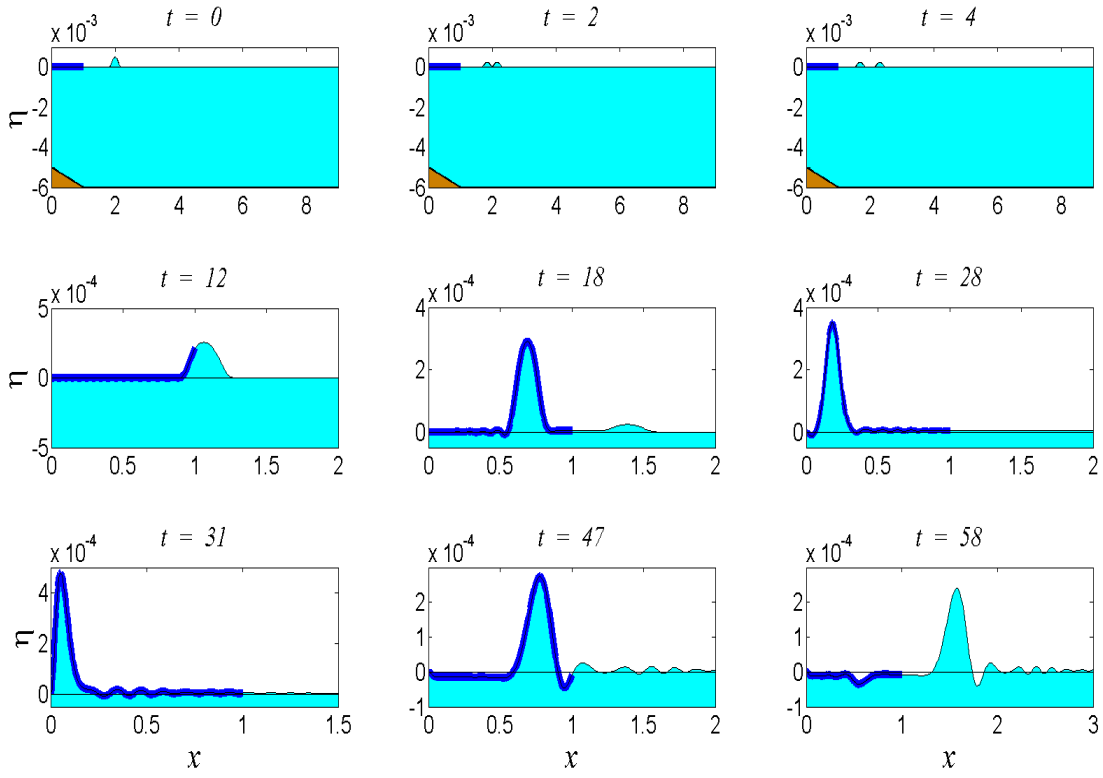

Figure 10. Calculated upper surface elevation at distinct moments. The elastic deformation of the strip is shown by using a thick blue line (the upper surface elevation is exaggerated).

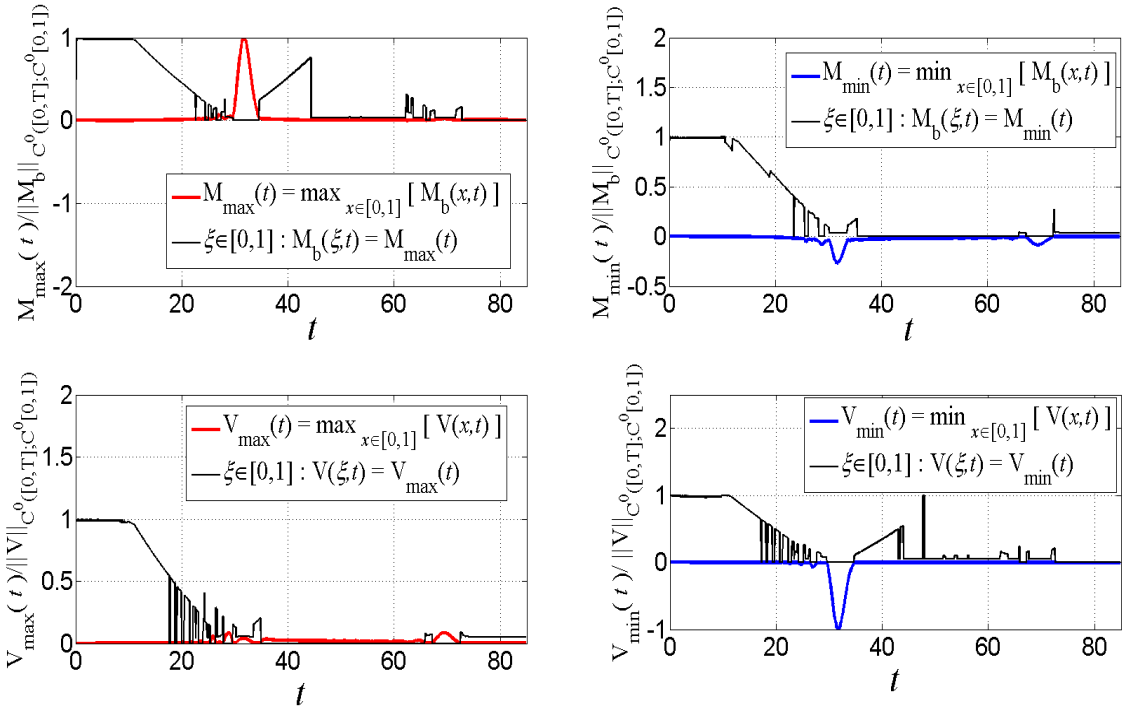

Figure 11. Extreme (max/min) values of bending moment and shear force and their location on the floating semi-fixed beam, in the case of second example.

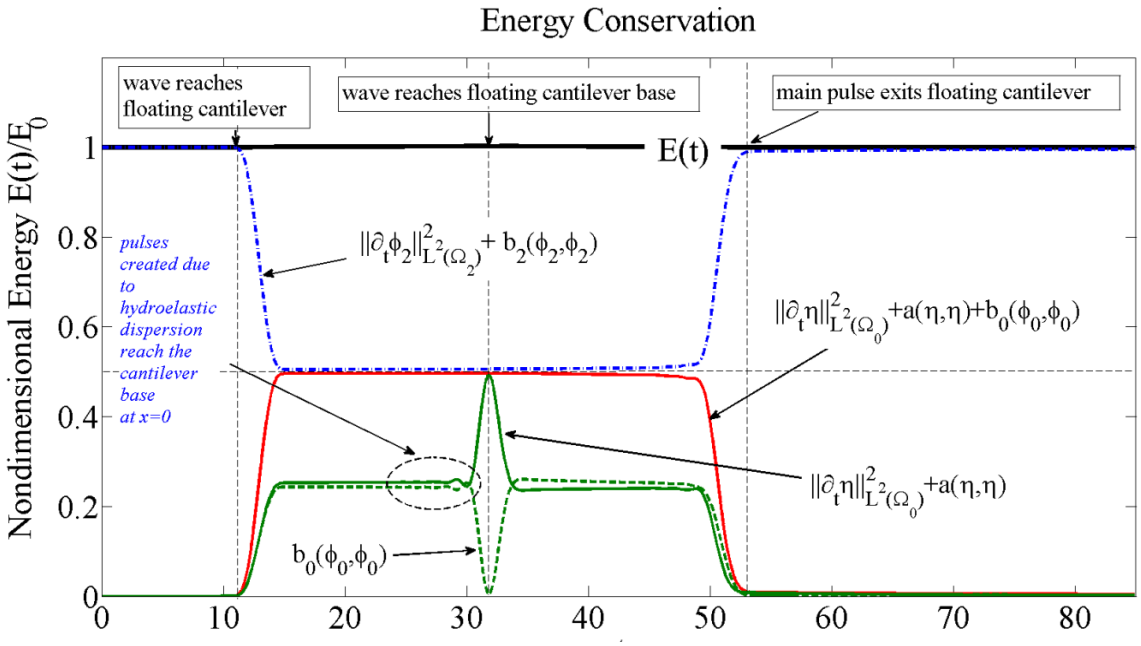

Figure 12. Energy conservation principle in the case of the semi-fixed floating beam.

In conclusion it must be noted that, although the present work is confined in two-dimensional large, elastic floating bodies under long-wave excitation, the whole methodology is directly extendable to two horizontal dimensions and more complex incident wave forms, finding useful applications in the study of more realistic phenomena of wave-elastic body interaction

in inhomogeneous environments. Additionally, extensions to include more general, shear deformable beam/plate models, effects of body finite depth effects and wave non-linearity is supported by the present model, and this is left to be examined in future work.

5. Conclusions

A new hydroelastic FEM model is presented for two-dimensional problems concerning the response of large floating elastic bodies, in inhomogeneous shallow water environment, characterized by variable bathymetry and thickness distribution. More specifically, two configurations have been modelled, concerning a freely floating strip representing an ice floe or a VLFS, and a semi-fixed floating beam, able to simulate representing wave-floating body interaction in shallow water conditions. The variational formulations of the above problems are derived, along with the energy conservation principles and the weak solution stability estimates. A special higher-order finite element method is developed and applied to the calculation of the numerical solution. Present theoretical results concerning the energy conservation principle are also verified, providing a valuable insight into the physical phenomenon investigated. An important aspect of the present method is the ability to provide useful information concerning the space-time distribution of bending moments, which are particularly important in the study of ice shelf and ice floe breakup mechanisms.

References

1. Bennetts GL, Squire VA. 2012 On the calculation of an attenuation coefficient for transects of ice-covered ocean. *Proc. R. Soc. A* **468**, 136-162.
2. Vaughan GL, Bennetts LG, Squire VA. 2009 The decay of flexural gravity waves in long sea ice transects. *Proc. R. Soc. A* **465**, 2785-2812.
3. Williams TD, Squire VA. 2004 Oblique scattering of pane flexural-gravity waves by heterogeneities in sea-ice. *Proc. R. Soc. A* **460**, 3469-3497.
4. Young IR, Zieger S, Bahanin V. 2011 Global Trends in Wind Speed and Wave Height, *Science* **332**, 451-455.
5. Stroeve JC, Markus T,Boisvert L, Miller J, Barrett A.2014 Changes in Arctic melt season and implications for sea ice loss, *Geophys. Res. Lett.* **41** (4), 1216-1225.
6. Cavalieri DJ, Parkinson CL. 2008 Antarctic sea ice variability and trends, 1979-2006, *J. Geophys. Res.* **113** (C7).
7. Brunt KM, Okal EA, MacAyeal D R. 2011 Antarctic ice shelf calving triggered by the Honsu (Japan) Earthquake and tsunami, March 2011. *J. Glaciol.* **57**, 785-788.
8. Dupont TK, Alley RB. 2005 Assesment of the importance of ice sheet buttressing to ice-sheet flow, *Geophys. Res. Lett.* **32** (4), L04503.
9. Skvarca P, Rack W, Rott H, Ibarzábal y Donángelo T. 1999 Climatic trend and the retreat and disintegration of ice shelves on the Antarctic Peninsula : an overview. *Polar Res.* **18**, 151-157.
10. Bromirski PD, Sergienko OV, MacAyeal DR. 2010 Transoceanic infragravity waves impacting Antarctic ice shelves. *Geophys. Res. Lett.* **37**, L02502.
11. MacAyeal DR *et al*. 2006 Transoceanic wave propagation links iceberg calving margins of Antarctica with storms in tropics and Northern Hemisphere. *Geophys. Res. Lett.* **33**, L17502.
12. Rosier SHR, Green JAM, Scourse JD, Winkelmann R. 2013 Modeling Antarctic tides in response to ice shelf thinning and retreat. *J. Geophys. Res.-Oceans* **14**,1-11.

13. Squire VA. 2007 Of ocean waves and sea-ice revisited. *Cold Reg. Sci.Technol*. **49**, 110-133.
14. Squire VA. 1993 The breakup of shore fast sea ice, *Cold Reg. Sci. Technol.* **21**, 211-218.
15. Evans, D. V. & Davies, T. V., 1968 Wave-ice interaction. Report No. 1313, Davidson Lab – Stevens Institute of Technology, New Jersey
16. Meylan MH, Squire VA. 1994 The response of ice floes to ocean waves. *J. Geophys. Res.* **99** ,899–900.
17. Meylan M H. 2002 Wave response of an ice floe of arbitrary geometry. *J. Geophys. Res.* **107**, 5-1-5-11. (doi:10.1029/2000jc000713).
18. Bhattacharjee J, Soares GC. 2012 Flexural gravity wave over a floating ice sheet near a vertical wall. *J. Eng. Math.* **75**, 29-48.
19. Brocklehurst P, Korobkin AA, Părău EI. 2010 Interaction of hydro-elastic waves with a vertical wall. *J. Eng. Math.* **68**, 215-231
20. Chakrabarti A. 2000 On the solution of the problem of scattering of surface-water waves by the edge of an ice cover. *Proc. R. Soc. A* **456**, 1087-1099.
21. Squire VA. 2008 Synergies Between VLFS Hydroelasticity and Sea Ice Reasearch. *Int. J. Offshore Polar Eng.* **18**, 1-13.
22. Chen XJ, Wu YS, Cui WC, Juncher Jensen J. 2006 Review of Hydroelasticity Theories for Global Response of Marine Structures. *Ocean Eng.* **33**, 439–457.
23. Watanabe E, Utsunomiya T, Wang CM. 2004 Hydroelastic Analysis of Pontoon-type VLFS: A Literature Survey. *Eng. Struct.* **26**, 245–256.
24. Ohmatsu, S. 2005 Overview: Research on Wave Loading and Responses of VLFS. *Mar. Struct.* **18**, 149–168.
25. Squire VA, Dugan JP, Wadhams P, Rottier PJ, Liu AK. 1995 Of ocean waves and sea-ice. *Annu. Rev. Fluid Mech.* **27**, 115–168.
26. Wang CM, Watanabe E, Utsunomiya T. 2008 *Very Large Floating Structures*. London: Taylor and Francis.
27. Kashiwagi MA. 1998 B-spline Galerkin scheme for calculating the hydroelastic response of a very large floating structure waves. *J. Mar Sci. Tech.* **3**, 37–49.
28. Eatock Taylor R, Ohkusu M. 2000 Green functions for hydroelastic analysis of vibrating free-free beams and plates. *Appl. Ocean Res.* **22**, 295–314.
29. Kim JW, Ertekin RC. 1998 An eigenfunction-expansion method for predicting hydroelastic behaviour of a shallow-draft VLFS. In: Kashiwagi M, Koterayama W, Ohkusu M, editors. *Proc. 2nd Int. Conf. Hydroelastic Marine Tech*, Fukuoka, Japan: RIAM.
30. Watanabe E, Utsunomiya T. 1996 Transient response analysis of a VLFS at airplane landing. In: Watanabe Y, editor. *Proc. Int. Workshop on Very Large Floating Structures*, Watanabe, E.), pp. 243-7, Hayama, Japan.
31. Watanabe E, Utsunomiya T, Tanigaki S. 1998 A transient response analysis of a very large floating structure by finite element method. *Structural Eng./Earthquake Eng(JSCE)***15**, 155–163.
32. Endo H. 2000 The behaviour of a VLFS and an airplane during takeoff/landing run in wave condition. *Mar. Struct.* **13**, 477–91.
33. Kashiwagi M. 2000 A time-domain mode-expansion method for calculating transient elastic responses of a pontoon-type VLFS. *J. Marine Sci. Technol.* **5**, 89–100.
34. Montiel F, Bennets LG, Squire VA. 2012 The transient response of floating elastic plates to wavemaker forcing in two dimensions. *J. Fluid Struct.* **28**, 416-433.
35. Sturova IV. 2009 Time- dependent response of a heterogeneous elastic plate floating on shallow water of variable depth. *J. Fluid Mech.* **637**, 305-325.

36. Sun H, Cui WC, Liu YZ, Liao SJ. 2003. Hydroelastic response analysis of mat-like VLFS over a plane slope in head seas. *China Ocean Eng.***17**, 315–326.
37. Utsunomiya T, Watanabe E, Nishimura N. 2001 Fast multipole algorithm for wave diffraction/radiation problems and its application to VLFS in variable water depth and topography. *Proc. 12th Int. Conf. Offshore Mech. & Arctic Eng*. OMAE 2001, Paper 5202, vol. 7, pp. 1–7.
38. Belibassakis KA, Athanassoulis GA. 2005 A Coupled mode Model for the Hydroelastic Analysis of Large Floating Bodies over Variable Bathymetry Regions. *J. Fluid Mech.* **531**, 221–249.
39. Belibassakis KA, Athanassoulis GA. 2006 A couple-mode technique for weakly non-linear wave interaction with large floating structures lying over variable bathymetry. *App. Ocean Res.* **28**, 59-76.
40. Athanassoulis GA, Belibassakis KA. 2009 A novel-coupled mode theory with application to hydroelastic analysis of thick, non-uniform floating bodies over general bathymetry. *J. of Eng. for the Maritime Environment* **223**, 419-437.
41. Masuda K, Ikoma T, Kobayashi A, Uchida M. 2003 Effect of Tsunami Wave Profile on the Response of a Floating Structure in Swallow Sea. *In Proc. 13th Int. Offshore and Polar Eng. Conf.* 1, pp. 381-384. Honolulu: ISOPE.
42. Masuda K, Miyazaki T, Takamura H. 1998 Study on estimation method for motions and mooring tensions of moored floating structure in offshore area under tsunami. *In Proc. 14th Ocean Engineering Symposium*, pp. 161–166.
43. Wen YK, Shinozuka M. 1972 Analysis of floating plate under ocean waves. *J Waterways, Harbors Coastal Eng. Div.* **98**, 177–90
44. Chen, X.J., Jensen, J.J., Cui, W.C. & Fu, S.X., 2003. Hydroelasticity of a floating plate in multidirectional waves. Ocean Eng. 30, 1997–2017.
45. Endo H, Yoshida K. 1998 Timoshenko Equation of Vibration for Plate-Like Floating Structures. *In Proc. of 2nd Int. Conf. on Hydroelasticity in Marine Technol.* pp. 255–264, Fukuoka, Japan.
46. Papathanasiou TK, Belibassakis KA. 2014 Hydroelastic analysis of VLFS based on a consistent coupled mode system and FEM. *The IES journal Part A: Civil and Structural Engineering* 7**(3)**, 195-206, Taylor & Francis.
47. Stoker J. 1957 *Water Waves: The mathematical Theory with Applications*, New York: Wiley-Interscience.
48. Brezis H. 1983 *Analyse Fonctionnelle, théorie et applications*, Paris: Masson.
49. Adams RA. 1975 *Sobolev Spaces*, New York: Academic Press.
50. Prenter PM. 1975 *Splines and variational methods*, J.Wiley & Sons.
51. Hughes JR. 2000 *The Finite ElementMethod: Linear Static and Dynamic Finite Element Analysis*, Dover Publications.
52. Okal EA, Synolakis C. 2003 A Theoretical Comparison of Tsunamis from Dislocations and Landslides, *Pure Appl. Geophys.* **160**, 2177-2188
53. Hammack JL. 1973 A note on Tsunamis: Their generation and propagation in an ocean of uniform depth, *J. Fluid Mech.* **60**, 769-799.
54. Drifting with Ice island B 31, *NASA Earth Observatory*, http://earthobservatory.nasa.gov/IOTD/view.php?id=83519 (accessed 21/8/2014)
55. Sergienko, OV. 2010 Elastic response of floating glacier ice to impact of long-period ocean waves, *J. Geophys. Res.***115**, F04028.